Journal of Materials Chemistry C

ROYAL SOCIETY OF CHEMISTRY

PAPER

View Article Online
View Journal

Cite this: DOI: 10.1039/d5tc03324a

Quantitative evaluation of mechanochromic luminescent materials under controlled grinding stimuli

Suguru Ito, *[a] Sayaka Nagai,[a] Minako Ikeya,[a] Takaki Mashimo,[b] Tomohiro Seki, [c] Hajime Ito, [bd] Yoshimitsu Sagara, [e] Toshiki Mutai, [f] Yousuke Ooyama [g] and Ken Nakano *[h]

Mechanochromic luminescent (MCL) materials have attracted growing attention owing to their potential applications in sensing, display, and security technologies. Although crystalline MCL materials have been the most intensively investigated, quantitative evaluation of their mechanical-stimuli-responsiveness remains challenging, particularly in powdered form. Herein, a custom-built apparatus is developed to monitor real-time emission color changes in crystalline powders of MCL materials under quantitatively controlled grinding stimuli. Time-dependent emission spectra obtained using this apparatus are analyzed using two newly defined parameters k_{prog} and k_{conv}. These parameters allow for quantitative comparison of the mechanical-stimuli-responsiveness of a series of organic and organometallic MCL materials with diverse structures and provide insights into their underlying mechanisms. Load-dependent measurements further suggest that mechanical force lowers the activation barrier for the collapse of the crystal structure. This methodology offers a general strategy for evaluating powdered MCL materials and contributes to the rational design and development of advanced MCL systems.

Received 5th September 2025,
Accepted 4th December 2025

DOI: 10.1039/d5tc03324a

rsc.li/materials-c

1. Introduction

Stimuli-responsive luminescent materials have attracted increased attention for next-generation optoelectronic and sensing technologies owing to their ability to convert external stimuli into optical signals.[1,2] Among various types of stimuli, mechanical force is especially important because it is ubiquitous in both natural and artificial environments, serves as a practical input signal for devices, and often needs to be detected or visualized. Mechanochromic luminescence (MCL) materials, which exhibit reversible changes in their solid-state photoluminescence color in response to mechanical stimuli, are promising candidates for applications such as pressure sensors, rewritable optical storage, and wearable devices.[2] A wide variety of MCL materials have been developed, including organic and organometallic crystals,[3–6] liquid crystals,[7] and polymers.[8] Among these, crystalline organic and organometallic compounds have been the most extensively studied. Their MCL behavior is typically evaluated by manually grinding powdered samples using a spatula or a mortar and pestle, which is an inherently qualitative approach. Given the increasing number and structural diversity of reported MCL materials, their mechano-responsive behaviors are expected to vary significantly. This clearly indicates the need for a quantitative methodology to evaluate and compare the responsiveness of powdered MCL materials to mechanical stimulation. Establishing such a methodology would accelerate the rational design and development of MCL systems.

Mechanical stimuli applied to crystalline materials include grinding, compressing, and smashing, which correspond to anisotropic pressure, isotropic pressure, and tensile force, respectively.[9] Tensile testing and compression testing are

[a] Department of Chemistry and Life Science, Graduate School of Engineering Science, Yokohama National University, 79-5 Tokiwadai, Hodogaya-ku, Yokohama 240-8501, Japan. E-mail: suguru-ito@ynu.ac.jp
[b] Division of Applied Chemistry and Frontier Chemistry Center, Faculty of Engineering, Hokkaido University, Sapporo, Hokkaido, Japan
[c] Department of Chemistry, Faculty of Science, Shizuoka University, Shizuoka City, Shizuoka 422-8529, Japan
[d] Institute for Chemical Reaction Design and Discovery (WPI-ICReDD), Hokkaido University, Sapporo, Hokkaido, Japan
[e] Department of Materials Science and Engineering, Institute of Science Tokyo, 2-12-1 Ookayama, Meguro-ku, Tokyo 152-8550, Japan
[f] Department of Materials and Environmental Science, Institute of Industrial Science, The University of Tokyo, 4-6-1, Komaba, Meguro-ku, Tokyo 153-8505, Japan
[g] Applied Chemistry Program, Graduate School of Advanced Science and Engineering, Hiroshima University, 1-4-1 Kagamiyama, Higashi, Hiroshima 739-8527, Japan
[h] Faculty of Environment and Information Sciences, Yokohama National University, 79-7 Tokiwadai, Hodogaya, Yokohama 240-8501, Japan. E-mail: nakano@ynu.ac.jp

widely used as standard methods to evaluate the mechanical strength of metals and polymers, both in academic research and industrial applications. However, these tests are not suitable for quantitatively evaluating how powdered samples respond to grinding stimuli. Notably, some crystalline MCL materials respond differently to grinding and compressing stimuli.[10] Therefore, a suitable method is required to quantitatively evaluate the responsiveness of crystalline MCL materials to grinding-type mechanical stimuli.

Several approaches have been reported to evaluate the mechanical-stimuli-responsiveness of crystalline MCL materials. Atomic force microscopy (AFM) has been employed to probe local mechanical responses of individual crystals at the nanoscale.[11] While valuable for examining surface deformation or local force-response behavior, AFM has limited capability in capturing differences in responsiveness arising from variations in crystal faces, particle size, or morphology, even within the same compound. From a practical perspective, evaluating the average responsiveness at the bulk level is preferable, since differences in the responsiveness of individual crystals are averaged out in bulk samples. To apply quantitative mechanical stimuli at the bulk-level, methods such as ball milling or manual grinding with a force gauge have been used.[12] However, these approaches are unsuitable for real-time monitoring of luminescence changes, thereby hindering detailed quantitative analysis of MCL behavior. A notable previous study demonstrated real-time monitoring of mechanoresponsive emission color changes using a custom-built setup, where quantitative grinding stimuli were applied by a pestle and analyzed *via* image processing, and the same instrumentation was applied to additional compounds.[13] While this image-processing approach can determine the threshold required to trigger an emission-color change, defining general and quantitative parameters for the progression of spectral change and the propensity for structural conversion would provide deeper insight into the responsiveness of diverse crystalline MCL materials to grinding stimuli.

Herein, we have developed a new apparatus that enables real-time monitoring of emission color changes in powdered MCL materials under quantitatively controlled grinding stimuli. In contrast to previously reported setups using a pestle, this system applies grinding stimuli *via* vertical loading and horizontal rotation to a sample sandwiched between two glass plates. Time-dependent emission spectra obtained using this setup were analyzed using two mechanical-stimuli-responsiveness constants established in this study, which enable evaluation of the progression of spectral change and the propensity for conversion from the initial crystalline state to another emissive state. These parameters were determined for eight organic and organometallic crystalline MCL materials **1–8** with diverse structures (Fig. 1), realizing quantitative comparison of their responsiveness to grinding stimuli. Furthermore, through load-dependent experiments, we demonstrate that structural transformation becomes more pronounced under stronger mechanical stimuli.

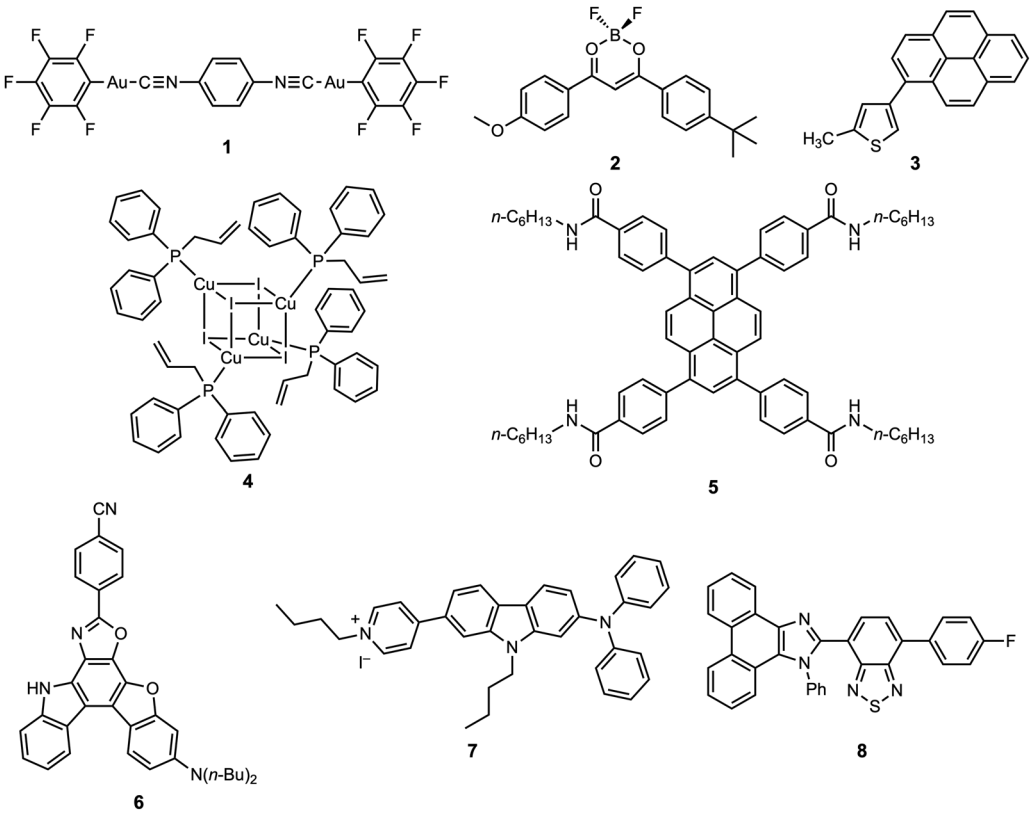

Fig. 1 Structures of MCL compounds **1–8** investigated in this study.

2. Materials and methods

2.1. Materials

All crystalline MCL materials **1–8** were prepared following previously reported procedures.[4f,g,i,6b,c,14] Their MCL properties were essentially the same as those reported in the literature, although slight deviations in the maximum emission wavelengths of crystalline or ground samples were observed.

2.2. Apparatus

A schematic diagram, photographs, and engineering drawings of the custom-built apparatus developed for applying quantitative grinding stimuli are shown in Fig. 2a–c and Fig. S1. The apparatus mainly consists of two parallel flat glass substrates, a metal plate, a rotating stage, and a stepping motor (Fig. 2a). Powdered samples are sandwiched between the two glass substrates. One of the glass substrates (outer diameter 40 mm, thickness 4 mm; OPB-40C04-P, OptoSigma) is mounted on the rotating stage (KS421-60, Suruga Seiki), and the other (outer diameter 25 mm, thickness 3 mm; OPB-25C03-P, OptoSigma) is fixed to the metal plate. The rotation speed of the stage is controlled by a stepping motor controller (D92, Suruga Seiki) connected to a handy terminal (D700, Suruga Seiki). The metal plate itself provides a vertical load of 2.4 N and moves smoothly along the vertical axis, guided by two vertical shafts and two linear bearings. Additional pairs of metal weights (2.4 N each) can be mounted onto the metal plate to increase the total vertical load. By adjusting both the vertical load and the rotation speed, mechanical stimuli equivalent to grinding can be quantitatively applied to the powdered samples (Fig. 2b).

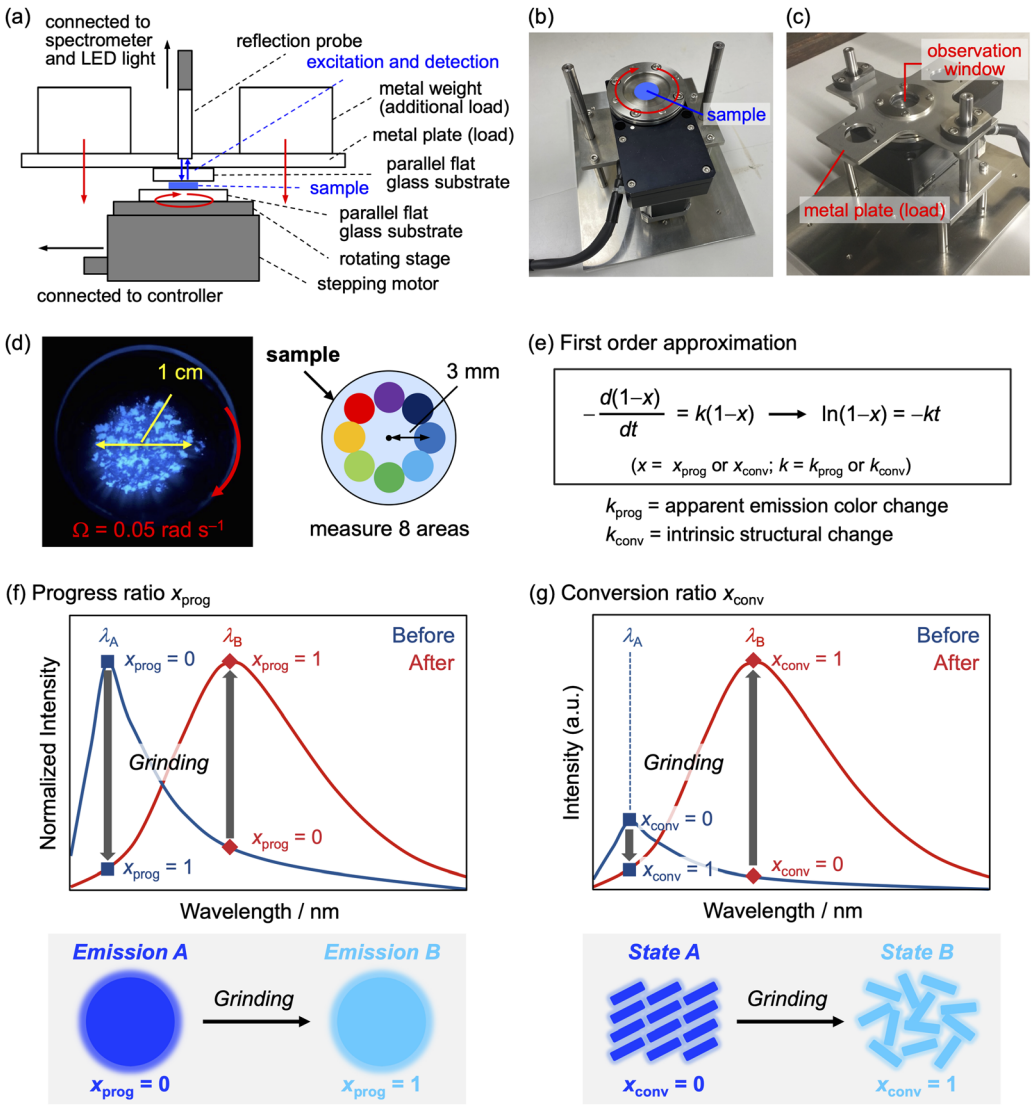

Fig. 2 (a)–(c) Apparatus for applying quantitative grinding stimuli to powdered samples. (a) Side view of the simplified schematic diagram. (b) Photograph showing the rotating stage. The metal plate is uncovered from the top. (c) Photograph taken from a diagonal angle. (d) Photograph of the powdered sample under 365 nm UV light, viewed through the observation window (left). Schematic representation of the measurement points on the sample (right). (e) Brief explanation of the responsiveness constants k_{prog} and k_{conv}. (f) and (g) Schematic illustration explaining the definitions of the progress ratio x_{prog} based on the emission-color change (f) and the conversion ratio x_{conv} based on the structural change (g).

Changes in emission color induced by this mechanical stimulus can be monitored in real time through an observation window at the top of the apparatus (Fig. 2c), using a commercial miniature fiber-optic spectrometer (FLAME-S-XR1-ES, Ocean Optics) equipped with a reflection probe (R400-7-SR, Ocean Optics), a 365 nm LED light source (LSM-365A, Ocean Optics), and an LED light controller (LDC-1, Ocean Optics).

2.3. Procedure

The specific experimental procedure is as follows. Powdered samples of crystalline MCL materials (*ca.* 1 mg) were placed at the center of the glass substrate and spread with a spatula to a diameter of *ca.* 1 cm (Fig. 2d, left). The samples on the substrate were then heated in an oven to restore the original emission color, as the emission color can slightly change due to partial crushing during the spreading process. The substrate with the sample was mounted on the rotating stage, and the other glass substrate attached to the metal plate was placed on top of the sample. The grinding stimulus is applied by rotating the bottom substrate at a constant angular velocity (Ω = 0.05 rad s^{-1}). At this low rate, frictional heating is expected to be negligible. Because the path length for one rotation is longer at larger radii, the stimulus is not homogeneous across the substrate by design. Therefore, the emission spectra were recorded at eight radial positions located 3 mm from the center of the sample (Fig. 2d, right), using the fiber-optic spectrometer at regular intervals. The probe (acceptance angle $\approx 25^\circ$) was positioned 2 mm above the surface of the glass substrate, corresponding to a probe-sample distance of 5 mm when the 3 mm glass thickness is included. With this geometry, the collection area is *ca.* 2.2 mm in diameter, and spectra from this area were recorded at each position.

2.4. Analysis of mechanical-stimuli-responsiveness

Based on the obtained spectra, the apparent progress of the emission color change and the intrinsic structural change of the crystal were analyzed using first-order approximations, from which the responsiveness constants k_{prog} and k_{conv} were determined (Fig. 2e).

2.4.1. Responsiveness constant k_{prog} derived from progress ratio x_{prog}. To analyze the responsiveness of emission color changes to grinding stimuli, the progress ratio x_{prog} is defined based on the intensity ratios R_A and R_B at the maximum emission wavelengths λ_A and λ_B before and after grinding (Fig. 2f). The intensity ratios $R_{A,before}$ and $R_{B,before}$ for the initial spectrum before grinding are given by:

$$R_{A,before} = \frac{I_{A,before}}{I_{A,before} + I_{B,before}} \quad (1)$$

$$R_{B,before} = \frac{I_{B,before}}{I_{A,before} + I_{B,before}} \quad (2)$$

where $I_{A,before}$ and $I_{B,before}$ represent the emission intensities at λ_A and λ_B, respectively, before grinding.

Similarly, the intensity ratios $R_{A,after}$ and $R_{B,after}$ for the spectrum after grinding are defined as:

$$R_{A,after} = \frac{I_{A,after}}{I_{A,after} + I_{B,after}} \quad (3)$$

$$R_{B,after} = \frac{I_{B,after}}{I_{A,after} + I_{B,after}} \quad (4)$$

The progress ratio x_{prog} at a given time t is then defined as:

$$x_{prog,t} = \frac{R_{A,t} - R_{A,before}}{R_{A,after} - R_{A,before}} = \frac{R_{B,t} - R_{B,before}}{R_{B,after} - R_{B,before}} \quad (5)$$

We assume that the progress rate of the spectral change in response to grinding stimuli depends only on the progress ratio x_{prog}. Specifically, the progress rate decreases as x_{prog} increases. Based on this assumption, the progress rate can be expressed as:

$$-\frac{d(1 - x_{prog})}{dt} = k_{prog}(1 - x_{prog}) \quad (6)$$

Here, k_{prog} is defined as the mechanical-stimuli-responsiveness constant representing the progress rate of spectral change. The integrated form of eqn (6) is:

$$\ln\left(\frac{1 - x_{prog,t}}{1 - x_{prog,0}}\right) = -k_{prog}t \quad (7)$$

where $x_{prog,0}$ and $x_{prog,t}$ represent the progress ratio at initial time t_0 and any given time t, respectively. Assuming $x_{prog,0}$ is 0, k_{prog} can be simplified as:

$$\ln(1 - x_{prog,t}) = -k_{prog}t \quad (8)$$

Accordingly, a plot of $\ln(1 - x_{prog})$ *versus* t should yield a straight line with a slope of $-k_{prog}$.

2.4.2. Responsiveness constant k_{conv} derived from conversion ratio x_{conv}. It should be noted that k_{prog} is focused on the ease of emission-color change in response to grinding stimuli. In other words, the progress ratio x_{prog}, used to determine k_{prog}, does not generally correspond to the conversion ratio x_{conv}, which represents the degree of transformation from the initial crystalline state A to the ground state B (Fig. 2g). The two ratios become identical ($x_{prog} = x_{conv}$) only under the conditions that the absolute emission intensity at the maximum emission wavelength remains unchanged before and after grinding ($I_{A,before} = I_{B,after}$), and the intensity ratios at the two wavelengths λ_A and λ_B are symmetric ($R_{A,before}/R_{B,before} = R_{B,after}/R_{A,after}$). If the emission intensity increases substantially after grinding, a significant spectral change may be observed even when a small fraction of the crystalline state A is converted to the amorphous state B ($x_{prog} > x_{conv}$). Therefore, the ease of conversion from state A to state B should be described by a different responsiveness constant k_{conv}, which is derived from the conversion ratio x_{conv}. Assuming that excited-state energy transfer from A to B is negligible, the emission intensity at λ_A

and λ_B at a given time t ($I_{A,t}$ and $I_{B,t}$) can be expressed as:

$$I_{A,t} = I_{A,\text{before}} \times \left(1 - x_{\text{conv},t}\right) + I_{B,\text{after}} \times \frac{R_{A,\text{after}}}{R_{B,\text{after}}} \times x_{\text{conv},t} \quad (9)$$

$$I_{B,t} = I_{A,\text{before}} \times \frac{R_{B,\text{before}}}{R_{A,\text{before}}} \times \left(1 - x_{\text{conv},t}\right) + I_{B,\text{after}} \times x_{\text{conv},t} \quad (10)$$

The intensity ratio at λ_A and λ_B at time t ($R_{A,t}$ and $R_{B,t}$) are then given by:

$$R_{A,t} = \frac{I_{A,t}}{I_{A,t} + I_{B,t}} \quad (11)$$

$$R_{B,t} = \frac{I_{B,t}}{I_{A,t} + I_{B,t}} \quad (12)$$

Substituting eqn (9) and (10) into eqn (11) yields:

$$R_{A,t} = \frac{C + Dx_{\text{conv},t}}{A + Bx_{\text{conv},t}} \quad (13)$$

where the coefficients are defined as:

$$A = \left(1 + \frac{R_{B,\text{before}}}{R_{A,\text{before}}}\right) \times I_{A,\text{before}}$$

$$B = \left(1 + \frac{R_{A,\text{after}}}{R_{B,\text{after}}}\right) \times I_{B,\text{after}} - \left(1 + \frac{R_{B,\text{before}}}{R_{A,\text{before}}}\right) \times I_{A,\text{before}}$$

$$C = I_{A,\text{before}}$$

$$D = \frac{R_{A,\text{after}}}{R_{B,\text{after}}} \times I_{B,\text{after}} - I_{A,\text{before}}$$

Rearranging eqn (13), the conversion ratio $x_{\text{conv},t}$ at time t can be determined by:

$$x_{\text{conv},t} = \frac{C - A \times R_{A,t}}{B \times R_{A,t} - D} \quad (14)$$

As in the case of k_{prog}, we assume that the conversion rate from the state A to B depends only on the amount of unconverted crystalline state A. The mechanical-stimuli-responsiveness constant k_{conv}, which describes the ease of conversion, is then expressed as:

$$\ln(1 - x_{\text{conv},t}) = -k_{\text{conv}}t \quad (15)$$

3. Results and discussion

3.1. Responsiveness constant k_{prog} of various MCL crystals

Mechanical stimuli applied during grinding can be divided into static pressure in the vertical direction and shear force in the horizontal direction. To apply these two types of forces in a controlled and reproducible manner, we developed a custom-built apparatus specifically designed for powdered MCL crystals. In this setup, the sample is sandwiched between two parallel glass substrates: the bottom substrate is mounted on a rotating stage, and the top one is fixed to a metal plate that provides vertical pressure. Static pressure is applied through the weight of the metal plate and can be increased by adding metal weights. Shear force is introduced by rotating the stage, which moves the lower glass substrate relative to the fixed upper one and shears the sample sandwiched between them.

Initially, [$(C_6F_5Au)_2$(μ-1,4-diisocyanobenzene)] (**1**)[6c] was selected as a model compound to evaluate the mechanical-stimuli responsiveness of the emission color using the developed apparatus, since its crystalline powder exhibits qualitatively high sensitivity to manual grinding. Under UV light irradiation (365 nm), the powdered crystals of **1** exhibit blue emission with a maximum emission wavelength (λ_{em}) at 440 nm (Fig. 3a–c). Upon amorphization by grinding, the emission color changes to yellow (λ_{em} = 548 nm). The original crystallinity and blue emission are restored by heating the ground sample at 100 °C.

Crystalline powders of **1** were sandwiched between two glass substrates in the apparatus, and quantitative grinding stimuli were applied using the weight of the metal plate and the rotation of the stage (Movie S1). The resulting emission changes were monitored through the observation window located at the top of the apparatus (Fig. 3a). The torque of the grinding stimuli depends on the distance from the center and the slight difference in the amount of the sample, which results in inhomogeneous changes of the sample. To minimize variations arising from sample inhomogeneity, emission spectra were recorded from eight radial positions in the sample at specified time intervals (0, 5, 15, 25, 50, 75, 100, 125, 150, 200, 300 s) (Fig. S2). For selected time points (0 s, 25 s, 100 s, 300 s), the spectra obtained at these eight positions are shown in Fig. 3b. The intensity of the blue emission gradually decreased, while that of the yellow emission increased over time. These spectral changes indicate that the MCL behavior of **1** originates from a transition between two distinct emissive states A and B. This observation is consistent with the previous report,[6c] in which the blue and yellow emissions of **1** were assigned to emissions from an intraligand-localized π–π* excited state and a ligand-to-Au–Au bond charge-transfer excited state, respectively.

Quantitative analysis of the emission spectra obtained under controlled grinding stimuli revealed the ease of emission color change in **1** through the determination of the responsiveness constant k_{prog}. The maximum emission wavelengths of **1** were 440 nm (λ_A) and 548 nm (λ_B) for the initial blue-emissive state A and the ground yellow-emissive state B, respectively (Fig. 3c). The intensity ratios $R_{440,\text{before}}/R_{548,\text{before}}$ and $R_{440,\text{after}}/R_{548,\text{after}}$ were 0.836 : 0.164 and 0.065 : 0.935, respectively. Based on these values, the progress ratio x_{prog} was calculated for all spectra (Table S1). A time-dependent plot of the averaged x_{prog} values measured at eight points is shown in Fig. 3d. In addition, values of $\ln(1 - x_{\text{prog}})$ were plotted against time t (Fig. 3e). The plot exhibits linear behavior up to 150 s, after which the data deviates from the straight line as x_{prog} approaches a plateau around 0.8. Contrary to the assumption that the responsiveness of spectral change to grinding stimuli depends solely on x_{prog}, the actual responsiveness of **1** appears to decrease as the amorphous region expands. In other words, the responsiveness of the crystalline material is most accurately

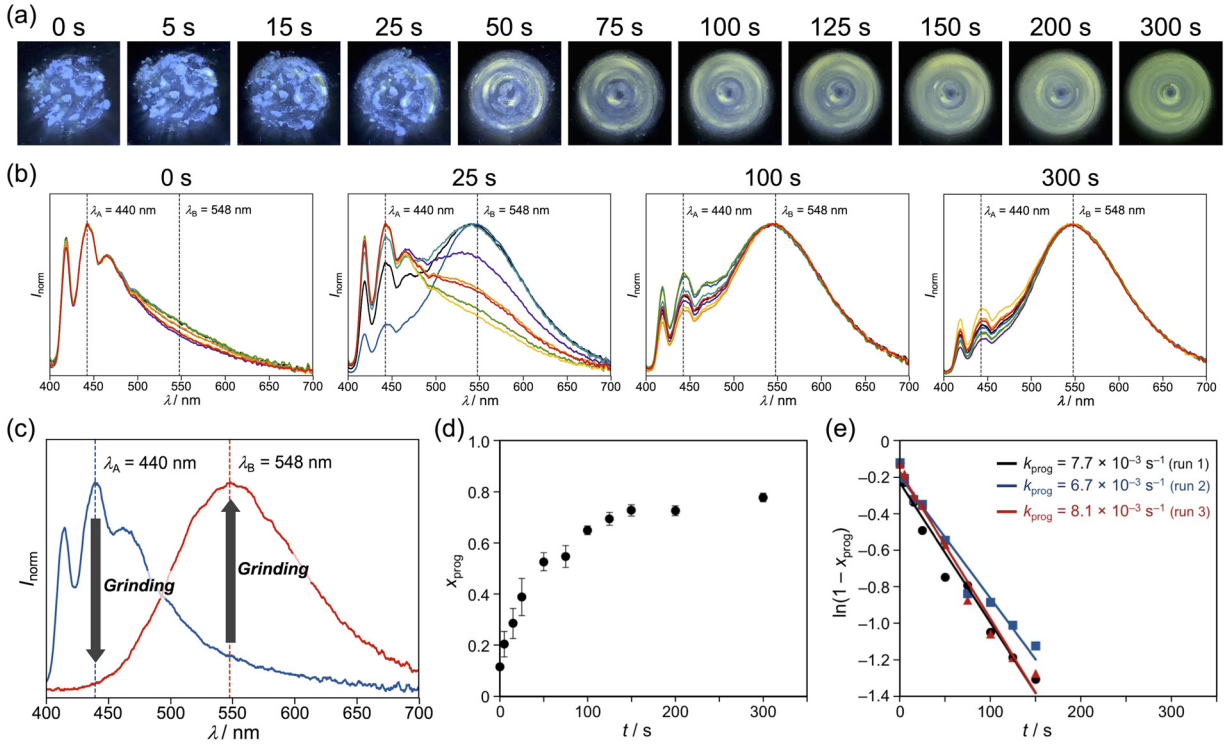

Fig. 3 (a) Photographs of **1** after certain time duration observed from the top window under UV light irradiation (365 nm). (b) Normalized emission spectra of **1** measured at eight points of the loaded sample at t = 0, 25, 100, and 300 s. (c) Normalized emission spectra of **1** in the initial crystalline (blue solid line) and ground amorphous (red solid line) states. (d) Time course of the averaged progress ratio x_{prog} of **1**. Each point represents the average of eight observation points, and error bars represent the standard error. (e) Plots of $\ln(1 - x_{prog})$ *versus* t for three independent experiments of **1**.

reflected in the initial linear region. The mechanical stimuli-responsiveness constant k_{prog} was thus determined from the slope of the linear fit up to 150 s, giving a value of 7.7 × 10^{-3} s^{-1}. The same experiment was repeated twice under identical conditions, yielding k_{prog} values of 6.7 × 10^{-3} and 8.1 × 10^{-3} s^{-1}. Averaging the results of the three experiments provided a $k_{prog,ave}$ value of 7.5 × 10^{-3} s^{-1} for **1**.

To investigate the relationship between structure and responsiveness, the mechanical-stimuli-responsiveness constants k_{prog} of additional organic and organometallic MCL materials **2–8** with diverse molecular structures were determined using the same experimental protocol as that applied for **1** (Table 1, Tables S2–S8 and Fig. 4a, Fig. S3–S18). Time-dependent emission spectra of **2–8** under quantitatively controlled grinding stimuli were recorded using the custom-built apparatus. Based on the characteristic patterns of spectral change during grinding, these compounds were classified into two categories: compounds **2** and **3** exhibited a clear decrease in one emission band accompanied by an increase in another (Fig. S3 and S4), while compounds **4–8** showed a gradual

Table 1 Maximum emission wavelengths, intensity ratios, and mechanical-stimuli-responsiveness constants of **1–8**[a]

Compound	λ_A[b] [nm]	λ_B[c] [nm]	$R_{A,before}/R_{B,before}$[d]	$R_{A,after}/R_{B,after}$[e]	$k_{prog,ave}$ [10^{-3} s^{-1}]	$I_{B,after}/I_{A,before}$[f]	$k_{conv,ave}$ [10^{-3} s^{-1}]
1	440	548	83.6 : 16.4	6.5 : 93.5	7.5	5.4	2.7
2	461	548	93.5 : 6.5	12.9 : 87.1	2.4	0.3	5.1
3	419	481	83.2 : 16.8	8.8 : 91.2	2.8	3.3	1.3
4	551	588	54.8 : 45.2	44.7 : 55.3	1.2	4.8	0.3
4[g]	551	588	54.8 : 45.2	44.7 : 55.3	3.2	4.8	1.0
4[h]	551	588	54.8 : 45.2	44.7 : 55.3	8.5	4.8	3.7
5	455	471	57.5 : 42.5	37.8 : 62.2	2.1	1.1	2.0
6	583	625	54.9 : 45.1	38.3 : 61.7	3.5	1.6	2.7
7	590	650	65.2 : 34.8	27.0 : 73.0	3.1	0.7	4.2
8	498	567	70.9 : 29.1	14.7 : 85.3	2.5	3.1	1.3

[a] Static pressure from the vertical direction was applied by metal plate (2.4 N). Shear force in the horizontal direction was applied by rotating glass plate at Ω = 0.05 rad s^{-1}. [b] Maximum emission wavelength of initial crystalline sample. [c] Maximum emission wavelength of manually ground sample. [d] Intensity ratio of the emission at λ_A and λ_B before grinding. [e] Intensity ratio of the emission at λ_A and λ_B after grinding. [f] Intensity ratio of the emission at λ_A before grinding and λ_B after grinding. [g] Two additional weights (2.4 N × 2) were used. [h] Four additional weights (2.4 N × 4) were used.

bathochromic shift in their emission maxima (Fig. 4b–e and Fig. S5–S9).

The spectral changes observed for the difluoroboron complex **2**[4f] and pyrenylthiophene **3**[14a] indicated a two-state transition behavior similar to that of **1** (Fig. S3 and S4). In both cases, the emission intensity from the initial crystalline state gradually decreased, while that from the amorphous state increased. Since both **2** and **3** are known to exhibit monomer emission in the crystalline state and excimer emission in the amorphous state,[4f,14a] the observed spectral changes can be rationalized by the absence of emissive intermediate states between the crystalline and amorphous states. From the slopes of linear fits to plots of $\ln(1 - x_{prog})$ *versus* time, the average mechanical-stimuli-responsiveness constants $k_{prog,ave}$ were estimated as 2.4×10^{-3} s^{-1} for **2** and 2.8×10^{-3} s^{-1} for **3** (Fig. 4a, Fig. S17b, c, S18b, c, and Table 1).

In contrast, compounds **4–8** showed a continuous bathochromic shift in emission maxima in response to grinding (Fig. 4b–e and Fig. S5–S9). According to previous reports, the emission-color change of Cu_4I_4 cluster complex **4** arises from local distortions in the crystal lattice that affect Cu–Cu distances.[6b] For tetramide **5**, the emission shift has been explained by the deviation of H-type columnar stacking.[4i] In addition, the mechanoresponsive emission changes in donor–π–acceptor-type compounds **6**[4g] and **7**,[14c] as well as the heteroaromatic donor–acceptor-type compound **8**,[14b] have been rationalized by planarization of molecular conformation and enhanced intermolecular interactions among polar molecules upon amorphization. These mechanistic interpretations account for the gradual spectral shifts of crystalline **4–8**, as the emission wavelengths of these MCL materials depend on the extent of the crystal structure destruction. Although the shifts in emission maxima were continuous, x_{prog} values were calculated from the intensity ratios R_A and R_B at the maximum emission wavelengths of the initial and ground states. The $k_{prog,ave}$ values were obtained from the slopes of linear fits to the plots of $\ln(1 - x_{prog})$ *versus* time (**4**: 1.2×10^{-3} s^{-1}; **5**: 2.1×10^{-3} s^{-1}; **6**: 3.5×10^{-3} s^{-1}; **7**: 3.1×10^{-3} s^{-1}; **8**: 2.5×10^{-3} s^{-1}; Fig. 4a, Fig. S17d–h, S18d–h, and Table 1). Among these, **6** exhibited the highest responsiveness, followed by **7**. These quantitative results are consistent with qualitative sensitivities observed under manual grinding and demonstrate that k_{prog} is a reliable quantitative metric for comparing the emission-color responsiveness of structurally diverse crystalline MCL materials.

3.2. Responsiveness constant k_{conv} of various MCL crystals

To quantitatively evaluate how readily the crystal structure of MCL materials collapses upon mechanical stimulation, the conversion rate constant k_{conv} was determined for compounds **1–8**. This analysis reinforces the previous discussion on k_{prog} by offering a more direct metric of structural disruption.

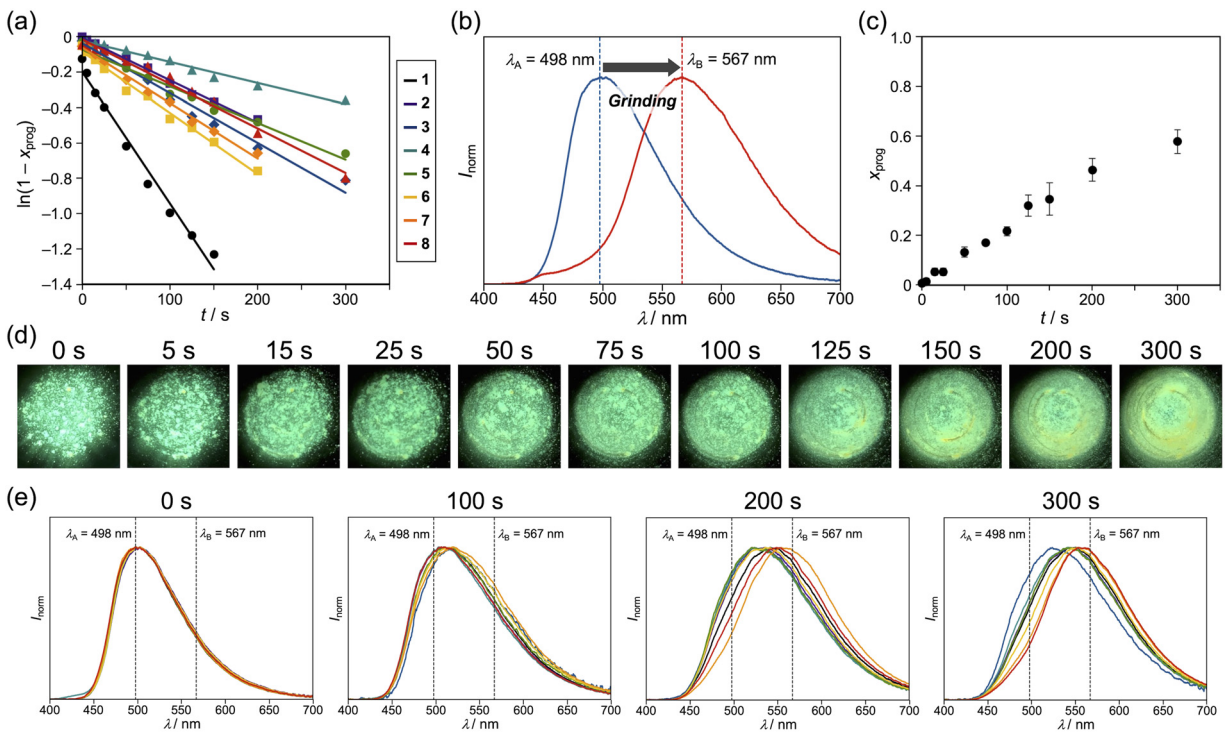

Fig. 4 (a) Plots of $\ln(1 - x_{prog})$ *versus* t for **1–8**. (b) Normalized emission spectra of **8** in the initial crystalline (blue solid line) and ground amorphous (red solid line) states. Maximum emission wavelengths λ_A (498 nm) and λ_B (567 nm) are denoted by dotted lines. (c) Time course of the averaged progress ratio x_{prog} of **8**. Each point represents the average of eight observation points, and error bars represent the standard error. (d) Photographs of **8** after certain time duration observed from the top window under UV light irradiation (365 nm). (e) Normalized emission spectra of **8** measured at eight points of the loaded sample at t = 0, 100, 200, and 300 s.

As detailed in Section 2.4.2, the determination of k_{conv} requires the emission intensities of both the initial crystalline state A and the fully ground state B. Therefore, their emission spectra were recorded under the same conditions as those used in the k_{prog} measurements (Fig. S19). From these data, the intensity ratios at the emission maxima of states A and B ($I_{B,after}/I_{A,before}$) were obtained for **1–8** (Table 1).

In the case of gold complex **1**, a significant increase in emission intensity was observed after grinding ($I_{548,after}/I_{440,before}$ = 5.4, Fig. 5a). Based on this value, the conversion ratio x_{conv} at each time point was calculated from the same time-dependent emission spectra used to determine k_{prog} (Fig. 5b and Table S1). By applying linear fitting to the plots of $\ln(1 - x_{conv})$ *versus* time, k_{conv} values of 2.7×10^{-3}, 2.3×10^{-3}, and 3.0×10^{-3} s^{-1} were obtained from three independent experiments (Fig. 5c), and the averaged value $k_{conv,ave}$ was 2.7×10^{-3} s^{-1} (Fig. 5d).

The same procedure was applied to determine the $k_{conv,ave}$ values for crystalline MCL compounds **2–8** (Fig. 5d, Fig. S20, S21 and Table 1, Tables S2–S8). For compounds **4–8**, which showed gradual bathochromic shifts in emission maxima upon grinding, intermediate emissive states likely exist between the crystalline state A and the fully ground state B. Nevertheless, $k_{conv,ave}$ was calculated under the assumption that the intensity ratios $R_{A,t}$ and $R_{B,t}$ reflect the conversion ratio $x_{conv,t}$. Notably, the order of k_{conv} values differed from that of k_{prog}, largely due to differences in the intensity ratios $I_{B,after}/I_{A,before}$. For example, while gold complex **1** exhibited the highest k_{prog} (7.5×10^{-3} s^{-1}), the k_{conv} of **1** was the third highest (2.7×10^{-3} s^{-1}), comparable to that of D–π–A-type compound **6** (2.7×10^{-3} s^{-1}). The high k_{prog} of **1** can thus be attributed primarily to its relatively high tendency toward amorphization (k_{conv} = 2.7×10^{-3} s^{-1}), and further enhanced by the substantial increase in emission intensity upon grinding ($I_{548,after}/I_{440,before}$ = 5.4).

The relationship between structural collapse and k_{conv} was further examined using powder X-ray diffraction (PXRD) data. Manual grinding of compounds **3** and **5–8** resulted in significant amorphization, as previously reported by PXRD analyses.[4i,g,14] The second highest k_{conv} (4.2×10^{-3} s^{-1}) of **7** suggests high structural fragility, while lower k_{conv} values (1.3×10^{-3} s^{-1}) of **3** and **8** indicate greater resistance to amorphization. Although the emission intensity of **7** decreased after grinding ($I_{650,after}/I_{590,before}$ = 0.7), this compound still exhibited the third highest k_{prog} among the compounds studied, highlighting that the high k_{conv} can compensate for intensity loss in determining k_{prog}.

In contrast, **2** and **4** retained significant crystallinity after grinding, as confirmed by PXRD analyses.[4f,6b] Nevertheless, **2** showed the highest k_{conv} (5.1×10^{-3} s^{-1}), likely because the emission observed after grinding originates from lattice defects formed within the crystalline phase. In this case, the high k_{conv} does not imply full amorphization but rather a high sensitivity of the crystal structure to defect formation sufficient to alter the emission properties. Conversely, the lowest k_{conv} of **4** (1.3×10^{-3} s^{-1}) reflects a relatively robust crystal structure. Although the emission intensity of **4** significantly increased after grinding ($I_{588,after}/I_{551,before}$ = 4.8), the low k_{conv} accounts for the lowest k_{prog} among the compounds examined.

3.3. Effect of vertical load

To investigate the relationship between applied vertical load and mechanical-stimuli-responsiveness, quantitative analysis

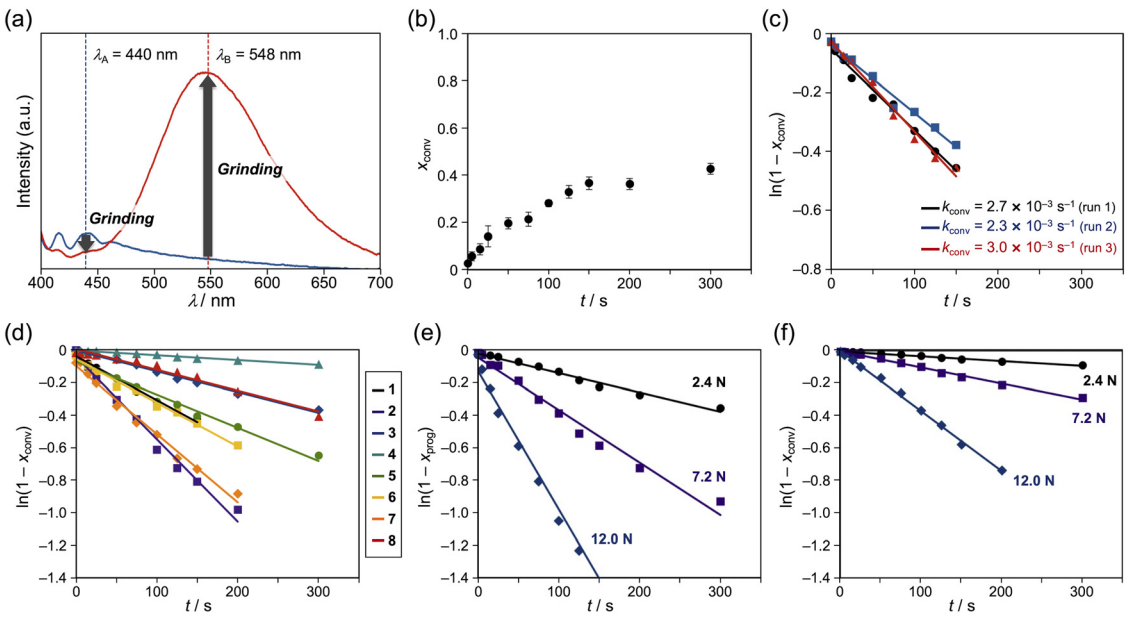

Fig. 5 (a) Emission spectra of **1** in the initial crystalline (blue solid line) and ground amorphous (red solid line) states. Maximum emission wavelengths λ_A (440 nm) and λ_B (548 nm) are denoted by dotted lines. (b) Time course of the averaged conversion ratio x_{conv} of **1**. Each point represents the average of eight observation points, and error bars represent the standard error. (c) Plots of $\ln(1 - x_{conv})$ *versus* t for three independent experiments of **1**. (d) Plots of $\ln(1 - x_{prog})$ *versus* t for **1–8**. (e) Plots of $\ln(1 - x_{prog})$ *versus* t of **4** with different vertical loads. (f) Plots of $\ln(1 - x_{conv})$ *versus* t of **4** with different vertical loads.

was performed under the conditions with additional weights using Cu cluster **4**, which exhibited the smallest values for both k_{prog} and k_{conv}. The vertical load was increased by placing one or two metal weights (2.4 N each) at both sides of the metal plate (2.4 N), resulting in a total applied load of 7.2 N and 12.0 N, respectively. Under these conditions, time-dependent emission measurements were conducted, from which the averaged rate constants $k_{prog,ave}$ and $k_{conv,ave}$ were determined to be 3.2×10^{-3} s^{-1} (7.2 N) and 8.5×10^{-3} s^{-1} (12.0 N) for $k_{prog,ave}$, and 1.0×10^{-3} s^{-1} (7.2 N) and 3.7×10^{-3} s^{-1} (12.0 N) for $k_{conv,ave}$, respectively (Fig. 5e, f, and Fig. S22–S25). The higher k_{prog} values compared to k_{conv} reflect the large increase in emission intensity after grinding ($I_{588,after}/I_{551,before}$ = 4.8).

The influence of applied load on the structural transformation was further evaluated by plotting $\ln k_{conv}$ against the applied load, which exhibited a linear relationship (Fig. S26). According to transition state theory, the activation free energy ($\Delta G^{\ddagger}$) is inversely proportional to the logarithm of the rate constant ($\ln k \propto -\Delta G^{\ddagger}$), suggesting that increasing mechanical load reduces the activation barrier required for crystal structure collapse. This observation is consistent with the Bell model,[15] in which mechanical force lowers $\Delta G^{\ddagger}$ as described by the equation $\Delta G^{\ddagger}(F) = \Delta G^{\ddagger}(0) - F{\cdot}x^{\ddagger}$. In this context, the slope of the $\ln k_{conv}$ *versus* force plot corresponds to $x^{\ddagger}$, providing a measure of the mechanical sensitivity of the structural transformation. In other words, increasing load indicates how effectively mechanical force accelerates structural transformation in crystalline MCL materials.

4. Conclusion

In summary, we have developed a new apparatus capable of applying quantitative grinding stimuli to powdered MCL materials while monitoring their emission spectral changes. This setup allows for the mechanistic differentiation of MCL behavior by determining whether the emission variation originates from a discrete transition between two emissive states or from continuous spectral shifts associated with gradual degradation of the crystal structure. To quantitatively evaluate the mechanical-stimuli-responsiveness of a wide range of crystalline MCL materials, two responsiveness constants k_{prog} and k_{conv} were defined. The constant k_{prog} represents the apparent progress of emission spectral change under grinding, whereas the constant k_{conv} reflects the grinding-stimuli-induced intrinsic conversion of the crystal structure to another disordered state. Notably, comparison between k_{conv} and PXRD patterns after manual grinding enabled evaluation of each material's tendency to undergo amorphization or defect generation, which are responsible for the observed luminescence changes. In addition, a linear correlation between applied load and $\ln k_{conv}$ supports a force-dependent reduction in the activation barrier for structural transformation, consistent with the Bell model.

The present analysis has focused on materials exhibiting red-shifted MCL between two states. Regarding applicability to other response behaviors, both k_{prog} and k_{conv} can be applied to blue-shifted responses. For luminescence quenching/enhancement responses, only k_{conv} can be formulated, since k_{prog} is defined from normalized spectral change. By contrast, multistep transitions are challenging and will require an extended formulation, which should be developed in future work.

Although individual crystallites may respond differently to mechanical forces, the use of powdered bulk samples under controlled conditions allows for the determination of averaged mechanical-stimuli-responsiveness parameters. Considering that practical applications of MCL materials will require bulk-scale processing, the quantitative evaluation method established in this study provides a foundation for the rational development of MCL systems with precisely tuned mechanical-stimuli-responsiveness.

Author contributions

S. I. conceived and designed the project, developed the analysis method, and wrote the manuscript with input from all authors. K. N. designed and developed the apparatus. S. N. and M. I. carried out the experiments. S. I., S. N., M. I., and K. N. analyzed the data. S. N., M. I., T. Ma., T. S., H. I., Y. S., T. Mu., and Y. O. prepared the samples. All authors discussed the results and approved the final version of the manuscript.

Conflicts of interest

The authors declare no competing financial interest.

Data availability

The data supporting this article have been included in the supplementary information (SI). Supplementary information: time-dependent luminescence spectra, photographs, supplementary data for determining responsiveness constants, supplementary data for effect of vertical load, and time course video (8× speed) of the luminescence color change of gold complex **1**. See DOI: https://doi.org/10.1039/d5tc03324a.

Acknowledgements

This work was partly supported by JSPS KAKENHI Grant Numbers JP17H06367, JP17H06370, JP18H04508, JP18H04520, and JP20H04665 in Grant-in-Aid for Scientific Research on Innovative Areas ''Soft Crystals: Area No. 2903'', JSPS KAKENHI Grant Number JP20K05645 within a Grant-in-Aid for Scientific Research (C), and JSPS KAKENHI Grant Number JP24K01451 within a Grant-in-Aid for Scientific Research (B). The authors appreciate Professor Kazuyuki Ishii (The University of Tokyo) for valuable discussions.

Notes and references

1 For reviews, see: (*a*) A. Fermi, *ChemPhotoChem*, 2025, **9**, e202400404; (*b*) Y. Shen, X. Le, Y. Wu and T. Chen, *Chem. Soc. Rev.*, 2024, **53**, 606; (*c*) M. Kato and K. Ishii, in *Soft Crystals*, ed. M. Kato and K. Ishii, Springer Nature, Singapore, 2023; (*d*) V. Kachwal and J.-C. Tan, *Adv. Sci.*, 2023, **10**, 2204848; (*e*) Y. Song, G. Pan, C. Zhang, C. Wang, B. Xu and W. Tian, *Mater. Chem. Front.*, 2023, **7**, 5104; (*f*) H. Zhou, J. Han, J. Cuan and Y. Zhou, *Chem. Eng. J.*, 2022, **431**, 134170; (*g*) S. Ito, *CrystEngComm*, 2022, **24**, 1112; (*h*) J. Zhang, B. He, Y. Hu, P. Alam, H. Zhang, J. W. Y. Lam and B. Z. Tang, *Adv. Mater.*, 2021, **33**, 2008071; (*i*) S. Xu, Y. Duan and B. Liu, *Adv. Mater.*, 2020, **32**, 1903530; (*j*) M. Kato, H. Ito, M. Hasegawa and K. Ishii, *Chem. – Eur. J.*, 2019, **25**, 5105.

2 For reviews, see: (*a*) R. Gavale, F. Khan and R. Misra, *J. Mater. Chem. C*, 2025, **13**, 1063; (*b*) X. Chen, J. Chen, X. Song, T. Du, X. Deng, Z. Deng, X.-G. Hu, X. Zeng, Z. Yang, H. Yang and R. Lan, *Adv. Mater.*, 2024, **36**, 2403766; (*c*) S. Nakamura, K. Hirano and N. Tohnai, *ChemPlusChem*, 2024, **89**, e202400437; (*d*) S. Ito, *J. Photochem. Photobiol., C*, 2022, **51**, 100481; (*e*) M. Jin and H. Ito, *J. Photochem. Photobiol., C*, 2022, **51**, 100478; (*f*) Y. Sun, Z. Lei and H. Ma, *J. Mater. Chem. C*, 2022, **10**, 14834; (*g*) F. Khan, A. Ekbote, G. Singh and R. Misra, *J. Mater. Chem. C*, 2022, **10**, 5024; (*h*) S. Ito, *Chem. Lett.*, 2021, **50**, 649; (*i*) X. Huang, L. Qian, Y. Zhou, M. Liu, Y. Cheng and H. Wu, *J. Mater. Chem. C*, 2018, **6**, 5075; (*j*) C. Wang and Z. Li, *Mater. Chem. Front.*, 2017, **1**, 2174; (*k*) Y. Sagara, S. Yamane, M. Mitani, C. Weder and T. Kato, *Adv. Mater.*, 2016, **28**, 1073.

3 For recent examples of organic crystalline MCL materials, see: (*a*) S. Ito, S. Wakiyama, H. Chen, M. Abekura, H. Uekusa, R. Ikemura and Y. Imai, *Angew. Chem., Int. Ed.*, 2025, **64**, e202422913; (*b*) C. Chen, Y. Guo, Z. Chang, K. Müllen and X.-Y. Wang, *Nat. Commun.*, 2024, **15**, 8555; (*c*) Y. Chen, A. Li, X. Li, L. Tu, Y. Xie, S. Xu and Z. Li, *Adv. Mater.*, 2023, **35**, 2211917; (*d*) L. Zhou, F. Ni, N. Li, K. Wang, G. Xie and C. Yang, *Angew. Chem., Int. Ed.*, 2022, **61**, e202203844; (*e*) H. Yu, X. Song, N. Xie, J. Wang, C. Li and Y. Wang, *Adv. Funct. Mater.*, 2021, **31**, 2007511; (*f*) C. Zhu, Q. Luo, Y. Shen, C. Lv, S. Zhao, X. Lv, F. Cao, K. Wang, Q. Song, C. Zhang and Y. Zhang, *Angew. Chem., Int. Ed.*, 2021, **60**, 8510; (*g*) L. He, R. Bai, R. Yu, X. Meng, M. Tian and X. Wang, *Angew. Chem., Int. Ed.*, 2021, **60**, 6013; (*h*) T. Nakae, M. Nishio, T. Usuki, M. Ikeya, C. Nishimoto, S. Ito, H. Nishihara, M. Hattori, S. Hayashi, T. Yamada and Y. Yamanoi, *Angew. Chem., Int. Ed.*, 2021, **60**, 22871; (*i*) Y. Gong, S. He, Y. Li, Z. Li, Q. Liao, Y. Gu, J. Wang, B. Zou, Q. Li and Z. Li, *Adv. Opt. Mater.*, 2020, **8**, 1902036; (*j*) Z. Wang, F. Yu, W. Chen, J. Wang, J. Liu, C. Yao, J. Zhao, H. Dong, W. Hu and Q. Zhang, *Angew. Chem., Int. Ed.*, 2020, **59**, 17580; (*k*) K. Zheng, F. Ni, Z. Chen, C. Zhong and C. Yang, *Angew. Chem., Int. Ed.*, 2020, **59**, 9972; (*l*) B. Li, B. Lawrence, G. Li and H. Ge, *Angew. Chem., Int. Ed.*, 2020, **59**, 3078; (*m*) T. Mutai, T. Sasaki, S. Sakamoto, I. Yoshikawa, H. Houjou and S. Takamizawa, *Nat. Commun.*, 2020, **11**, 1824.

4 For seminal examples of organic crystalline MCL materials, see: (*a*) J. Wang, J. Mei, R. Hu, J. Z. Sun, A. Qin and B. Z. Tang, *J. Am. Chem. Soc.*, 2012, **134**, 9956; (*b*) Y. Dong, B. Xu, J. Zhang, X. Tan, L. Wang, J. Chen, H. Lv, S. Wen, B. Li, L. Ye, B. Zou and W. Tian, *Angew. Chem., Int. Ed.*, 2012, **51**, 10782; (*c*) Y. Ooyama and Y. Harima, *J. Mater. Chem.*, 2011, **21**, 8372; (*d*) X. Luo, J. Li, C. Li, L. Heng, Y. Q. Dong, Z. Liu, Z. Bo and B. Z. Tang, *Adv. Mater.*, 2011, **23**, 3261; (*e*) S.-J. Yoon, J. W. Chung, J. Gierschner, K. S. Kim, M.-G. Choi, D. Kim and S. Y. Park, *J. Am. Chem. Soc.*, 2010, **132**, 13675; (*f*) G. Zhang, J. Lu, M. Sabat and C. L. Fraser, *J. Am. Chem. Soc.*, 2010, **132**, 2160; (*g*) Y. Ooyama, Y. Kagawa, H. Fukuoka, G. Ito and Y. Harima, *Eur. J. Org. Chem.*, 2009, 5321; (*h*) J. Kunzelman, M. Kinami, B. R. Crenshaw, J. D. Protasiewicz and C. Weder, *Adv. Mater.*, 2008, **20**, 119; (*i*) Y. Sagara, T. Mutai, I. Yoshikawa and K. Araki, *J. Am. Chem. Soc.*, 2007, **129**, 1520.

5 For recent examples of organometallic crystalline MCL materials, see: (*a*) T. Seki and R. Ishikawa, *Chem. – Eur. J.*, 2025, **31**, e202404241; (*b*) X. Zhang, J.-X. Song, X. Chang, K. Li and Y. Chen, *Chem. – Eur. J.*, 2024, **30**, e202304224; (*c*) A. M. T. Muthig, O. Mrózek, T. Ferschke, M. Rödel, B. Ewald, J. Kuhnt, C. Lenczyk, J. Pflaum and A. Steffen, *J. Am. Chem. Soc.*, 2023, **145**, 4438; (*d*) A. I. Solomatina, E. E. Galenko, D. O. Kozina, A. A. Kalinichev, V. A. Baigildin, N. A. Prudovskaya, J. R. Shakirova, A. F. Khlebnikov, V. V. Porsev, R. A. Evarestov and S. P. Tunik, *Chem. – Eur. J.*, 2022, **28**, e202202207; (*e*) A. Y. Baranov, E. A. Pritchina, A. S. Berezin, D. G. Samsonenko, V. P. Fedin, N. A. Belogorlova, N. P. Gritsan and A. V. Artem'ev, *Angew. Chem., Int. Ed.*, 2021, **60**, 12577; (*f*) Y. Dong, J. Zhang, A. Li, J. Gong, B. He, S. Xu, J. Yin, S. H. Liu and B. Z. Tang, *J. Mater. Chem. C*, 2020, **8**, 894; (*g*) T. Seki, K. Ida, H. Sato, S. Aono, S. Sakaki and H. Ito, *Chem. – Eur. J.*, 2020, **26**, 735.

6 For seminal examples of organometallic crystalline MCL materials, see: (*a*) B. Xu, Z. Chi, X. Zhang, H. Li, C. Chen, S. Liu, Y. Zhang and J. Xu, *Chem. Commun.*, 2011, **47**, 11080; (*b*) S. Perruchas, X. F. L. Goff, S. Maron, I. Maurin, F. Guillen, A. Garcia, T. Gacoin and J.-P. Boilot, *J. Am. Chem. Soc.*, 2010, **132**, 10967; (*c*) H. Ito, T. Saito, N. Oshima, N. Kitamura, S. Ishizaka, Y. Hinatsu, M. Wakeshima, M. Kato, K. Tsuge and M. Sawamura, *J. Am. Chem. Soc.*, 2008, **130**, 10044.

7 (*a*) X. Zhang, L. Li, Y. Chen, C. Valenzuela, Y. Liu, Y. Yang, Y. Feng, L. Wang and W. Feng, *Angew. Chem., Int. Ed.*, 2024, **63**, e202404202; (*b*) S. Zhang, C. Sun, J. Zhang, S. Qin, J. Liu, Y. Ren, L. Zhang, W. Hu, H. Yang and D. Yang, *Adv. Funct. Mater.*, 2023, **33**, 2305364; (*c*) M. Kondo, M. Hashimoto, S. Miura and N. Kawatsuki, *Mol. Cryst. Liq. Cryst.*, 2017, **644**, 78; (*d*) B. Huitorel, Q. Benito, A. Fargues, A. Garcia, T. Gacoin, J.-P. Boilot, S. Perruchas and F. Camerel, *Chem. Mater.*, 2016, **28**, 8190; (*e*) M. Mitani, S. Ogata, S. Yamane, M. Yoshio, M. Hasegawa and T. Kato, *J. Mater. Chem. C*, 2016, **4**, 2752; (*f*) M. Mitani, S. Yamane, M. Yoshio, M. Funahashi and T. Kato, *Mol. Cryst. Liq. Cryst.*, 2014, **594**, 112; (*g*) Y. Sagara and T. Kato, *Angew. Chem., Int. Ed.*,

2011, **50**, 9128; (*h*) Y. Sagara, S. Yamane, T. Mutai, K. Araki and T. Kato, *Adv. Funct. Mater.*, 2009, **19**, 1869; (*i*) V. N. Kozhevnikov, B. Donnio and D. W. Bruce, *Angew. Chem., Int. Ed.*, 2008, **47**, 6286; (*j*) Y. Sagara and T. Kato, *Angew. Chem., Int. Ed.*, 2008, **47**, 5175.

8 (*a*) S. Shimizu, J. M. Clough, C. Weder and Y. Sagara, *Angew. Chem., Int. Ed.*, 2025, **64**, e202510114; (*b*) Z.-P. Song, J. Wei, J. Liu, Z.-F. Chu, J.-X. Hu, S. Chakraborty, Y. Ma, B.-X. Li, Y.-Q. Lu and Q. Zhao, *Adv. Mater.*, 2025, **37**, 2419640; (*c*) D. J. Kiebala, R. Style, D. Vanhecke, C. Calvino, C. Weder and S. Schrettl, *Adv. Funct. Mater.*, 2023, **33**, 2304938; (*d*) S. Thazhathethil, T. Muramatsu, N. Tamaoki, C. Weder and Y. Sagara, *Angew. Chem., Int. Ed.*, 2022, **61**, e202209225; (*e*) R. Hertel, W. Maftuhin, M. Walter and M. Sommer, *J. Am. Chem. Soc.*, 2022, **144**, 21897; (*f*) H. Hu, X. Cheng, Z. Ma, R. P. Sijbesma and Z. Ma, *J. Am. Chem. Soc.*, 2022, **144**, 9971; (*g*) T. Muramatsu, Y. Okado, H. Traeger, S. Schrettl, N. Tamaoki, C. Weder and Y. Sagara, *J. Am. Chem. Soc.*, 2021, **143**, 9884; (*h*) M. Raisch, W. Maftuhin, M. Walter and M. Sommer, *Nat. Commun.*, 2021, **12**, 4243; (*i*) F. Hoshino, T. Kosuge, D. Aoki and H. Otsuka, *Mater. Chem. Front.*, 2019, **3**, 2681; (*j*) M. Gon, K. Kato, K. Tanaka and Y. Chujo, *Mater. Chem. Front.*, 2019, **3**, 1174; (*k*) C. Calvino, Y. Sagara, V. Buclin, A. P. Haehnel, A. del Prado, C. Aeby, Y. C. Simon, S. Schrettl and C. Weder, *Macromol. Rapid Commun.*, 2019, **40**, 1800705; (*l*) A. Kobayashi, Y. Yoshida, M. Yoshida and M. Kato, *Chem. – Eur. J.*, 2018, **24**, 14750; (*m*) Y. Sagara, M. Karman, E. Verde-Sesto, K. Matsuo, Y. Kim, N. Tamaoki and C. Weder, *J. Am. Chem. Soc.*, 2018, **140**, 1584; (*n*) S. Kato, K. Ishizuki, D. Aoki, R. Goseki and H. Otsuka, *ACS Macro Lett.*, 2018, **7**, 1087; (*o*) T. Sumi, R. Goseki and H. Otsuka, *Chem. Commun.*, 2017, **53**, 11885; (*p*) O. Toma, M. Allain, F. Meinardi, A. Forni, C. Botta and N. Mercier, *Angew. Chem., Int. Ed.*, 2016, **55**, 7998; (*q*) Q. Benito, X. F. Le Goff, S. Maron, A. Fargues, A. Garcia, C. Martineau, F. Taulelle, S. Kahlal, T. Gacoin, J.-P. Boilot and S. Perruchas, *J. Am. Chem. Soc.*, 2014, **136**, 11311; (*r*) B.-C. Tzeng, T.-Y. Chang, S.-L. Wei and H.-S. Sheu, *Chem. – Eur. J.*, 2012, **18**, 5105; (*s*) J. Lott and C. Weder, *Macromol. Chem. Phys.*, 2010, **211**, 28; (*t*) B. R. Crenshaw, M. Burnworth, D. Khariwala, A. Hiltner, P. T. Mather, R. Simha and C. Weder, *Macromolecules*, 2007, **40**, 2400; (*u*) M. Kinami, B. R. Crenshaw and C. Weder, *Chem. Mater.*, 2006, **18**, 946; (*v*) B. R. Crenshaw and C. Weder, *Chem. Mater.*, 2003, **15**, 4717; (*w*) C. Löwe and C. Weder, *Adv. Mater.*, 2002, **14**, 1625.

9 L. Wang, K. Wang, B. Zou, K. Ye, H. Zhang and Y. Wang, *Adv. Mater.*, 2015, **27**, 2918.

10 (*a*) Y. Liu, Q. Zeng, B. Zou, Y. Liu, B. Xu and W. Tian, *Angew. Chem., Int. Ed.*, 2018, **57**, 15670; (*b*) K. Nagura, S. Saito, H. Yusa, H. Yamawaki, H. Fujihisa, H. Sato, Y. Shimoikeda and S. Yamaguchi, *J. Am. Chem. Soc.*, 2013, **135**, 10322.

11 (*a*) J. P. Calupitan, A. Brosseau, P. Josse, C. Cabanetos, J. Roncali, R. Métivier and C. Allain, *Adv. Mater. Interfaces*, 2022, **9**, 2102246; (*b*) M. Yamashita, S. Nagai, S. Ito and T. Tachikawa, *J. Phys. Chem. Lett.*, 2021, **12**, 7826; (*c*) M. Louis, C. Piñero García, A. Brosseau, C. Allain and R. Métivier, *J. Phys. Chem. Lett.*, 2019, **10**, 4758; (*d*) D. Genovese, A. Aliprandi, E. A. Prasetyanto, M. Mauro, M. Hirtz, H. Fuchs, Y. Fujita, H. Uji-I, S. Lebedkin, M. Kappes and L. De Cola, *Adv. Funct. Mater.*, 2016, **26**, 5271.

12 (*a*) S. Ito, K. Fukuhara, N. Arakawa, S. Suzuki and Y. Imai, *Chem. – Eur. J.*, 2025, **31**, e202501677; (*b*) S. Ito, R. Sekine, M. Munakata, M. Yamashita and T. Tachikawa, *Chem. – Eur. J.*, 2021, **27**, 13982; (*c*) T. Sagawa, F. Ito, A. Sakai, Y. Ogata, K. Tanaka and H. Ikeda, *Photochem. Photobiol. Sci.*, 2016, **15**, 420; (*d*) T. Seki, T. Ozaki, T. Okura, K. Asakura, A. Sakon, H. Uekusa and H. Ito, *Chem. Sci.*, 2015, **6**, 2187; (*e*) Y. Ooyama, N. Yamaguchi, S. Inoue, T. Nagano, E. Miyazaki, H. Fukuoka, I. Imae, K. Komaguchi, J. Ohshita and Y. Harima, *Tetrahedron*, 2012, **68**, 529.

13 (*a*) P. W. McDonald, J. Xu, D. R. Lonsdale, I. Jones, B. Poggi, R. P. Cox, S. Aloise, A. D. Scully, C. Allain, L. Bodelot, S. A. Moggach, T. D. M. Bell, R. Métivier, S. G. B. Furness, L. Goerigk and C. Ritchie, *J. Mater. Chem. C*, 2024, **12**, 19371; (*b*) B. Poggi, L. Bodelot, M. Louis, R. Métivier and C. Allain, *J. Mater. Chem. C*, 2021, **9**, 12111.

14 (*a*) M. Ikeya, G. Katada and S. Ito, *Chem. Commun.*, 2019, **55**, 12296; (*b*) S. Nagai, M. Yamashita, T. Tachikawa, T. Ubukata, M. Asami and S. Ito, *J. Mater. Chem. C*, 2019, **7**, 4988; (*c*) Y. Ooyama, Y. Oda, Y. Hagiwara, H. Fukuoka, E. Miyazaki, T. Mizumo and J. Ohshita, *Tetrahedron*, 2013, **69**, 5818.

15 (*a*) A. Boscoboinik, D. Olson, H. Adams, N. Hopper and W. T. Tysoe, *Chem. Commun.*, 2020, **56**, 7730; (*b*) E. Evans and K. Ritchie, *Biophys. J.*, 1997, **72**, 1541; (*c*) G. I. Bell, *Science*, 1978, **200**, 618.